Journal of Catalysis **182,** 136–147 (1999)
Article ID jcat.1998.2307, available online at http://www.idealibrary.com on IDEAL®

Synthesis, Characterization, and Thiophene Desulfurization Activity of Unsupported γ-Mo_2N Macrocrystalline Catalysts

Eric J. Markel,*[,1] Susan E. Burdick,*[,2] Marion E. Leaphart II,* and Kenneth L. Roberts†[,3]

*Department of Chemical Engineering, University of South Carolina, Columbia, South Carolina 29208; and †Department of Chemical Engineering, North Carolina A&T State University, 330 McNair Hall, Greensboro, North Carolina 27411-0001

Received June 19, 1998; revised October 2, 1998; accepted October 12, 1998

Macrocrystals of γ-Mo_2N were synthesized by temperature-programmed reaction of macrocrystalline MoO_3 and NH_3 or N_2/H_2 mixtures. X-ray diffraction analyses indicate macrocrystalline Mo_2N is an aggregate of particles in crystallographic alignment with diameters ranging from 4.6 to 18 nm, depending on synthesis conditions. Scanning tunneling microscopy (STM) supports these observed diameters. Based on diffraction data and surface area measurements, it is concluded that the particles in each sample are found with a range of diameters, each flattened in the [200] direction with either an amorphous surface phase or polycrystalline interior. The highest crystal BET surface area achieved is 44 m^2/g. TGA was used to monitor the temperature-programmed reaction of MoO_3 and N_2/H_2 mixtures. The lowest reduction temperatures were observed in syntheses employing high H_2 concentrations and slow temperature ramping rates. The rate of the Mo_2N macrocrystal synthesis reaction was observed to be slower than the equivalent powder reaction, which could possibly be attributed to the effects of solid-state diffusion. The specific thiophene hydrodesulfurization (HDS) activity (units of mol/s m^2) of the Mo_2N macrocrystalline catalyst at 673 K was found to be higher than the powder form by a factor of 2.5. Weight-specific HDS activities and reaction product fractions over Mo_2N macrocrystal and powder catalysts were roughly the same. An analysis of reaction products over a range of conversions indicates thiophene desulfurizes to form predominantly 1-butene with smaller amounts of other C_4 hydrocarbons also present.

INTRODUCTION

γ-Mo_2N powders have been synthesized previously by several groups using temperature-programmed reaction of MoO_3 and NH_3 (1–3) or N_2/H_2 mixtures (4, 5). The high specific surface area of the Mo_2N powders could make them particularly promising catalysts for many industrial and environmental applications. γ-Mo_2N prepared by this method has been studied as a catalyst for NH_3 decomposition (6, 7), CO hydrogenation (8), ethane hydrolysis (8, 9), hydrodenitrogenation (10, 11), and hydrodesulfurization (12, 13) reactions. γ-Mo_2N powder is a highly porous, dark metallic-gray material composed of small particles (or crystallites) of micrometer-scaled proportions (5).

This work details the previously unreported analysis of Mo_2N macrocrystals for the hydrodesulfurization (HDS) reaction of thiophene. γ-Mo_2N macrocrystals are relatively small, dark metallic-gray platelets of moderately porous material which have visible dimensions varying from micrometer- to centimeter-scaled proportions. Macrocrystalline Mo_2N catalysts could be useful for several reasons including providing lower pressure drops in a packed bed reactor, being more amenable to study by advanced microscopic techniques such as scanning tunneling microscopy (5), and could possibly be more selective for industrial hydrodesulfurization reactions (14). Crystalline Mo_2N also may serve as the starting point for a range of crystal chemistries: Mo_2N powder can also be readily converted to carbides, borides, and metal using high temperature treatments in CH_4, BH_3, and H_2, respectively (10).

Previous work reported from this group has examined the effects of reaction parameters such as temperature, reactant gas composition, and water content on the synthesis of high surface area molybdenum nitride powders (7) and the reactivity of the unsupported Mo_2N catalysts for the NH_3 decomposition and thiophene HDS reactions (4, 12). Hydrogen lean mixtures of N_2 and H_2 were observed to produce mixtures of low surface area (10 m^2/g) material composed of MoO_2, Mo_2N, and Mo for the temperature-programmed reaction (7). This result combined with supporting temperature ramping experimental data indicates that at temperatures between 573 and 873 K MoO_2 is a possible intermediate of the temperature-programmed reaction. MoO_2 and molybdenum oxynitride have previously been reported as possible intermediates in the formation of Mo_2N powders for the temperature-programmed reaction systems containing MoO_3 and NH_3 (1).

[1] Current address: Exxon Polymer Research Center, 5200 Bayway Drive, Baytown, TX 77520.

[2] Current address: Department of Chemical Engineering, Texas A&M University, College Station, TX 77843-3122.

[3] To whom correspondence should be addressed. Fax: (336)334-7904. E-mail: kroberts@ncat.edu.

0021-9517/99 $30.00

The hydrodesulfurization of thiophene over Mo_2N powders has been previously reported by this group to produce butane as one of the initial products of the thiophene desulfurization reaction at 673 K (12). Significant amounts of butadiene and butene products and small amounts of tetrahydrothiophene were also reported to form during the desulfurization of thiophene. Sulfided Mo_2N catalysts were observed to have much higher area specific activities for the thiophene desulfurization reaction compared with supported sulfided cobalt/molybdenum catalysts. Mo_2N catalysts were not observed to be significantly affected by a combination of sulfiding for 4 h in a 10% H_2S in H_2 mixture and subsequent kinetic analysis for 12–18 h at 673 K as observed from subsequent X-ray diffractometry and Raman spectroscopy analyses. At temperatures above 773 K, some MoS_2 was observed as a result of the sulfiding process.

The surface areas of Mo_2N catalyst powders were varied from 6.0 to 108 m^2/g using a range of temperature rates and a variety of preparation conditions. The area specific HDS activity of the catalysts was observed to increase with significant decreases in surface area. Promotion of specific HDS activity for the low surface area catalysts was attributed to the detected presence of MoN in the catalyst samples.

REVIEW

Volpe and Boudart (1) were the first to report the production of high surface area γ-Mo_2N in temperature programmed reactions of MoO_3 in flowing NH_3. Subsequently, it was shown that ammonia decomposes during temperature-programmed synthesis and that high surface areas could also be achieved using N_2/H_2 mixtures as feed (4, 5). The reaction requires a slow temperature ramping rate (0.6 K/min from 298 to 980 K) and a high gas space velocity (typically 150,000 h^{-1}) through a packed bed of powdered MoO_3 to produce surface areas up to 170 m^2/g. These reaction conditions have been found to lead to MoO_3 reduction temperatures as low as 620 K. Reactions with high space velocity, low heating rate, and low synthesis temperatures produce the desired high surface area (3, 4).

The MoO_3 reduction reactions which produce high surface areas are termed topotactic because the γ-Mo_2N product has a well defined three-dimensional crystallographic orientation relative to the parent MoO_3 crystallite. Specifically, selected area electron diffraction data indicate that the (010) planes of MoO_3 are parallel to the (100) planes of product γ-Mo_2N. X-ray diffraction and electron diffraction data show that the powdered γ-Mo_2N product consists of micrometer-sized porous platelet aggregates of 3- to 4-nm-diameter crystallites in crystallographic alignment (1). Thus, the platelet morphology of MoO_3 is preserved in topotactic Mo_2N.

Because the reduction of MoO_3 to γ-Mo_2N is topotactic, the removal of oxygen and infusion of nitrogen must occur in a manner such that each intermediate reaction step is also topotactic. In this way, structural symmetry between the molybdenum lattice points exists throughout the entire reaction. Bertrand and Dufour (15) studied the topotactic isothermal reduction of MoO_3 to MoO_2 in flowing H_2 at 100 Torr (1 Torr = 133.3 N/m^2). Low temperatures (723–743 K) were used to avoid complete reduction of the oxides to Mo metal and water-free H_2 was used because slight traces of water have been shown to enhance MoO_3 sublimation by the formation of volatile hydrates (16):

$$MoO_3 + H_2 = MoO_2 + H_2O. \quad [1]$$

Using the selected area electron diffraction it was shown that the following structural relationships exist during the topotactic reduction: $[\bar{1}00]MoO_2 \parallel [010]MoO_3$, $[122]MoO_2 \parallel [100]MoO_3$, and $[12\bar{2}]MoO_2 \parallel [001]MoO_3$. The authors reported an activation energy of 19 ± 2 kcal/mol for this reduction.

Hillis, Kemball, and Roberts (17) studied the isothermal reduction of low surface area MoO_2 in flowing, atmospheric H_2 at temperatures from 543 to 788 K to form moderate surface area molybdenum metal:

$$MoO_2 + 2H_2 = Mo + 2H_2O. \quad [2]$$

The reaction product was identified by X-ray diffraction as a mixture of Mo metal and the low surface area MoO_2 starting material. At 723 K, the reduction kinetics were such that a period of 12 h was required for a 1% conversion to Mo. At equilibrium, it is expected that all of the molybdenum dioxide be converted to the metal (18). The specific surface area of the MoO_2/Mo product mixtures increased linearly from 2 m^2/g to a final value of 50 m^2/g. Possible topotactic relationships of the reactants and products were not addressed.

Solid structures. MoO_3 forms a crystalline solid with an ReO_3-type layered structure and an orthorhombic Bravais lattice (0.392 nm, 1.394 nm, 0.366 nm) (19). The layered planes are composed of corner sharing MoO_6 octahedra which are parallel to the (010) plane of the primitive cell. The Mo–O bond distance varies from 0.188 to 0.245 nm in each octahedron (20). Only weak physical interactions bind adjoining MoO_3 layers. MoO_2 has a monoclinic structure, with $a_o = 0.5584$ nm, $b_o = 0.4842$ nm, $c_o = 0.5608$ nm, and $b = 120°59'$ (20). The Mo–O bond length varies from 0.19 to 0.21 nm in MoO_2; the Mo–Mo bond length is 0.248 nm. In γ-Mo_2N, the Bravais lattice is face centered cubic, with $a_o = 0.4165$ nm (21). Each molybdenum atom is octahedrally surrounded by six nonmetallic sublattice sites. One Mo atom is present at $\frac{1}{2}, \frac{1}{2}, \frac{1}{2}$ and nitrogen is statistically distributed over the octahedral interstitial sites of the metallic sublattice as positions $\frac{1}{2}, 0, \frac{1}{2}$; $\frac{1}{2}, \frac{1}{2}, 0$; $0, \frac{1}{2}, \frac{1}{2}$; $1, \frac{1}{2}, \frac{1}{2}$; $\frac{1}{2}, 1, \frac{1}{2}$; and $\frac{1}{2}, \frac{1}{2}, 1$ as required to maintain a stoichiometric ratio. Using these

parameters, the separation of Mo–Mo atoms in γ-Mo_2N is 0.2945 nm, and the Mo-N separation is 0.208 nm (20).

EXPERIMENTAL

Catalyst synthesis. Crystalline Mo_2N was synthesized from macrocrystals of MoO_3. These starting macrocrystals were produced from MoO_3 powder (Johnson Matthey, 99.999%) using high temperature sublimation. Approximately 100 g of MoO_3 powder was loaded into a silica quartz semicylindrical boat, placed into a sealed 2-inch-diameter silica combustion tube and heated in a large Lindberg furnace under flowing nitrogen gas. As the MoO_3 powder sublimated at temperatures above 500°C, product MoO_3 macrocrystals were deposited at the opposite end of the combustion tube and maintained at room temperature. After the complete sublimation of the powder MoO_3, the furnace was cooled and the MoO_3 macrocrystalline product was removed.

Approximately 25.0 g of MoO_3 macrocrystals was loaded into a quartz boat and placed in a combustion tube and connected to an NH_3 (Matheson, 99.9999%) source. The transparent yellow crystals obtained exhibit the flat platelet habit on MoO_3 and were typically more than 1 cm long, 3–5 mm wide, and less than 200 μm thick. Similar results were obtained using 75% H_2/25% N_2 mixtures (Matheson, N_2, 99.9995%, and H_2, 99.9995%). The sample was heated to 980 K at 0.6 K/min in NH_3 flowing at 0.001 m^3/min. At the end of the temperature program, the sample was removed from the furnace and cooled without exposure to oxygen. The cooled sample is air-sensitive and must be passivated before removal to the atmosphere. Passivation of the Mo_2N macrocrystals was accomplished by stopping the ammonia flow and allowing air to contact the sample through 0.5 m of 0.635-cm-i.d. tube for 48 h. Previous work in this group has found that an amorphous MoO_2 surface layer forms on the surface of passivated γ-Mo_2N powders from diffuse reflectance FTIR and indicated by XRD measurements (22). Previous work has shown that substantial losses in surface area accompany the passivation procedure (1).

Molybdenum nitride powder was synthesized using methods previously reported (4). Approximately 0.1 g of MoO_3 powder was loaded into a quartz tube fitted with a porous ceramic frit and reacted in flowing NH_3 or N_2/H_2 at atmospheric pressures, using gas flow procedures and the temperature program methods described above. After the reaction was completed, the reactant gas was allowed to continue flowing and the Mo_2N powder was cooled to room temperature. After cooling, the reactant gas flow was halted and the solid product was passivated using air that contacted the product sample through 0.5 m of 0.635-cm-i.d. tubing for 24 h.

Characterization. Catalysts were characterized both before and after thiophene reaction using X-ray diffraction and BET surface area analysis. The fresh, unused catalysts were passivated and exposed to air before analysis. Fresh macrocrystalline catalysts were also examined using SEM and STM analyses. The "used" catalysts were treated in a 2.7% thiophene in hydrogen mixture and heated from room temperature to 673 K in the flowing mixture at 0.125 K/s. The flowing thiophene/hydrogen mixture was maintained at 0.5 ml/s over the bed of catalyst particles with variable superficial space velocity for a period of 24 h. Following the kinetic analysis, the catalysts were cooled to room temperature and exposed to air.

X-ray diffraction analysis. A Rigaku Model D-max-B single-axis diffractometer equipped with a Cu source operating at 20 mA and 30 kV was used for both powder and macrocrystal analyses. The detector was equipped with a monochromator for the rejection of all but the Cu$K\alpha$ line. All data were compared to JCPDS values for identification (20). Diffraction peak width data were analyzed to determine particle size using the Scherrer equation (23).

A special holder was designed to perform analyses of macrocrystals using the single-axis goniometer. The holder allowed the (100), (010), (001), and (111) planes of Mo_2N macrocrystal samples to be aligned in the direction parallel to the sample plane in the goniometer (Fig. 1), thus allowing one-dimensional analyses of Mo_2N macrocrystals in a powder diffractometer. Mo_2N macrocrystal samples were mounted into the holder using double-sided tape with minor alignment corrections performed with the samples in place in the goniometer.

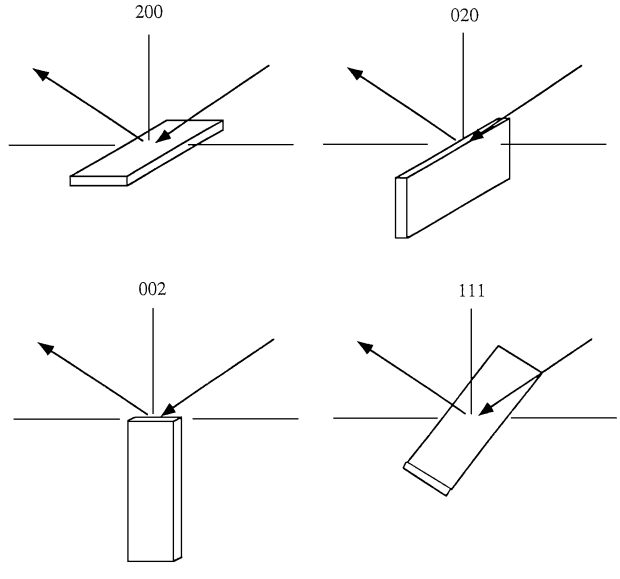

FIG. 1. Orientation of Mo_2N macrocrystal in goniometer stage for one-dimensional X-ray diffraction studies. The characteristic flat platelet morphology of MoO_3 is retained in the Mo_2N macrocrystal with the (200) plane of Mo_2N parallel to the basal (010) plane of MoO_3.

Surface area analysis. BET surface area analysis was performed using a Micromeritics 2700 dynamic adsorption analyzer. The N_2/He mixtures used in adsorption measurements were prepared in the laboratory by mixing high purity gases (Matheson, N_2, 99.9995%, and He, 99.9995%) in a Sierra electronic dual-channel mass flow controller. An integrating thermal conductivity detector was used to determine test gas composition during adsorption/desorption. Adsorption was carried out at 77 K.

Scanning electron microscopy. A Hitachi Model S2500 Delta microscope was used for SEM analyses. Crystalline Mo_2N samples were mounted on SEM stubs for analysis by evaporating a small portion of solution containing a dilute aqueous suspension of the dispersed crystals. Solution concentrations over several orders of magnitude were tested to optimize particle density on the stub.

Scanning tunneling microscopy. Analyses were performed using a Digital Nanoscope II system equipped with a 1- by 1- by 0.3-μm scan head and platinum tip. A single crystal of topotactic Mo_2N was mounted onto the scan head using carbon paste. The top layers of the macrocrystals could be easily peeled away using adhesive tape to reveal a fresh, clean surface for analysis.

Thermogravimetric analysis. Mo_2N syntheses were also performed using a thermogravimetric analyzer (Perkin-Elmer TGA7). Typically, 25 mg of MoO_3 macrocrystals or powder were loaded into a platinum sample pan for analysis. A gas–liquid feed system allowed for the programmed addition of high purity (>99.99%) nitrogen, hydrogen, water, helium, and a mixture of 1.0% oxygen in nitrogen for passivation purposes. It should be noted that careful system purging both before and after reaction must be exercised in these experiments involving hydrogen in the presence of oxygen and platinum. The analyzer was clamped shut to prevent opening in the event of a power failure. It should be noted that hydrogen is produced by catalytic decomposition of NH_3 during Mo_2N synthesis in NH_3 (4) and that appropriate purges are necessary in syntheses employing NH_3.

Thiophene desulfurization kinetic measurements. Thiophene desulfurization rates were measured in a continuous flow, fixed-bed reactor described previously (12). The reactor was constructed of 1/8″-i.d. quartz tubing and contained a bed of 0.100 g of catalyst. Each experimental run was begun by heating the catalyst from room temperature to 673 K in the 2.7% thiophene in hydrogen mixture at 0.125 K/s. The thiophene/hydrogen mixture flowed at 0.5 ml/s over the bed of catalyst particles with a superficial space velocity of 15 s^{-1}. Products were identified by gas chromatography and mass spectrometry (GC/MS) using a Hewlett Packard 5890 gas chromatograph connected in series to a Finnigan Mat ITD mass spectrometer. Reaction products were quantified using the above-mentioned gas chromatograph equipped with a flame ionization detector (FID) and a Graphpac GC column (Alltech, Inc.) for the analysis of HDS reaction products. After allowing a 20-min stabilization period at 673 K, the analytical system automatically sampled and analyzed the reaction products every 20 min over a 12-h period. Afterward, the reactant mixture flow rate was increased from 0.5 ml/s to 1.0, 2.0, 3.33, and 6.66 ml/s to decrease residence time and approach differential conversion operation. Several analyses were obtained at each elevated flow rate for each catalyst. Comparison studies were carried out using the procedures mentioned above using Mo_2N powder catalysts.

RESULTS

Macrocrystal synthesis. The crystalline MoO_3 starting material has a flat needle morphology typically 1 cm long, 3–5 mm wide, and less than 200 μm thick. During reaction, the transparent macrocrystals darken, starting at the edges until the entire solid is black. Following complete reduction, nitridation, and passivation, the product has a dark metallic luster and is quite flexible. Gross macrocrystal morphology appears to be unchanged.

The reduction/nitridation reaction of MoO_3 macrocrystals with 75% H_2 in N_2 was investigated using thermogravimetric analysis (TGA). During temperature programmed reaction at 0.6 K/min (Fig. 2), reaction commences at 650 K with a total mass loss of 28%, corresponding to that expected for the complete conversion of MoO_3 to Mo_2N. Reduction of MoO_3 powder occurs at much lower temperatures. The TGA profiles do not plateau at any discrete intermediate compositions. X-ray diffraction analyses of the intermediate compositions show the presence of small amounts of low surface area MoO_2 as well as a solid phase previously reported (1, 4) but not fully characterized with lattice planes at 205 pm. This result from TGA

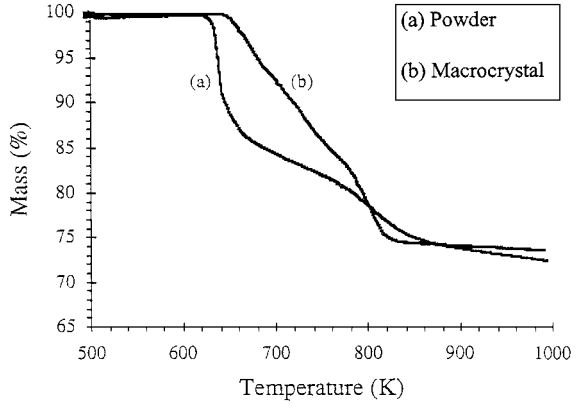

FIG. 2. Thermogravimetric analysis of temperature-programmed reaction of MoO_3 powder and macrocrystals in 85% H_2 in nitrogen. Total mass change corresponds to conversion of MoO_3 to Mo_2N.

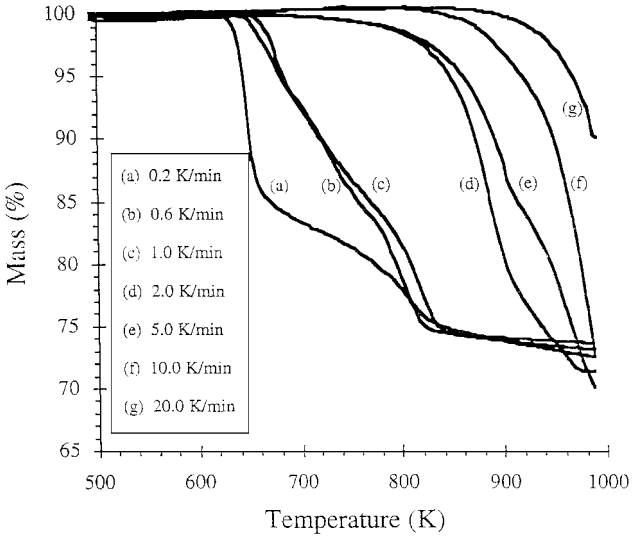

FIG. 3. Effect of temperature ramping rate on crystalline MoO_3 reduction/nitridation.

TABLE 1

Summary of Particle Sizes Calculated from X-ray Diffraction Peak Widths Using the Scherrer Equation for Mo and Mo_2N Crystal Products

Gas composition	Temp. ramping rate (K/min)	D [111] (nm)	D [200] (nm)	S_g [111] (m^2/g)	S_g [200] (m^2/g)
75% H_2	0.2	7.4	6.3	85	101
75% H_2	0.6	8.4	6.9	76	92
75% H_2	1	9.6	6.9	66	92
75% H_2	2	14.3	7.6	44	82
75% H_2	5	17.9	8.6	35	73
75% H_2	10	—	18.2		34
75% H_2	20	—			
10% H_2	0.6	13.6	9.8	46	64
20% H_2	0.6	13.0	9.0	49	70
40% H_2	0.6	12.3	8.0	51	79
60% H_2	0.6	11.4	7.8	55	81
85% H_2	0.6	9.6	6.9	66	92
100% H_2	0.6	—	—	—	—
100% NH_3	0.6	5.6	4.6	113	137

experiments differed from that observed for air exposed passivated powder Mo_2N catalysts, both of which did not indicate the presence of MoO_2 in the bulk catalyst phase by means of XRD analysis. This result agrees with previous reports that passivation gas composition can significantly influence the structural properties for the synthesis of Mo_2N unsupported catalysts (24). Because the sample mass is continuously changing throughout reaction, the solid transforms through a continuum of states either involving mixtures of stoichiometric compounds or involving nonuniform, defect (nonstoichiometric) compositions (3).

At higher temperature ramping rates (Fig. 3), reaction occurs at successively higher temperatures using analogous temperature programs for each MoO_3 macrocrystal sample. In most cases, the final product of reaction is Mo_2N, with some small amounts of residual MoO_3 and Mo observed at higher ramping rates, as identified by XRD analysis. Previous work with Mo_2N powders reported that the highest surface areas are produced in syntheses with low reduction temperatures (25). We were unable to accurately measure the surface areas of the material produced in the TGA due to the small sample sizes available but X-ray linewidth data point to a steady drop in product surface area with increasing temperature ramping rate (Table 1).

A range of gas compositions were also tested (Fig. 4). Lower reduction temperatures are observed at the higher hydrogen contents, as is observed in the powder system (22). In pure hydrogen, MoO_3 reduces at a relatively low temperature to form molybdenum metal. In all other cases, the product of reaction as determined by TGA mass change and X-ray diffraction is γ-Mo_2N. Analysis of Mo_2N X-ray linewidths indicates that low temperatures yield higher surface area material (Table 1).

Macrocrystal characterization. Scanning electron microscopy (Fig. 5) reveals the layered platelet habit of the Mo_2N macrocrystals. This layering is seen in the gross morphology as well as in the terraced features at the edges of the macrocrystals and in samples which have fractured, cleaving along the principal crystallographic planes to yield thin flakes. The layered habit is an artifact of the MoO_3 starting material. Mo_2N does not have an intrinsic layer structure because it is symmetric along all three crystallographic axes.

Small flat platelets or flakes approximately the size of typical powdered MoO_3 crystallites (<1 mm thick) are observed at the surface of some Mo_2N macrocrystals (Fig. 6). The platelets possibly form when reduced material forms at the edge of a relatively thin (<10 mm) macrocrystal and

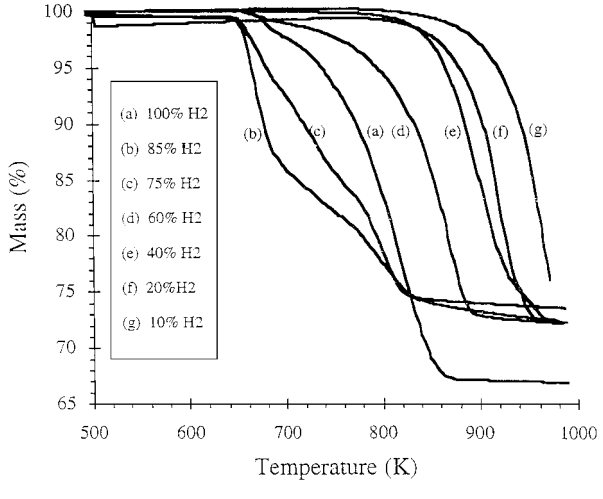

FIG. 4. Effect of gas composition on crystalline MoO_3 reduction/nitridation.

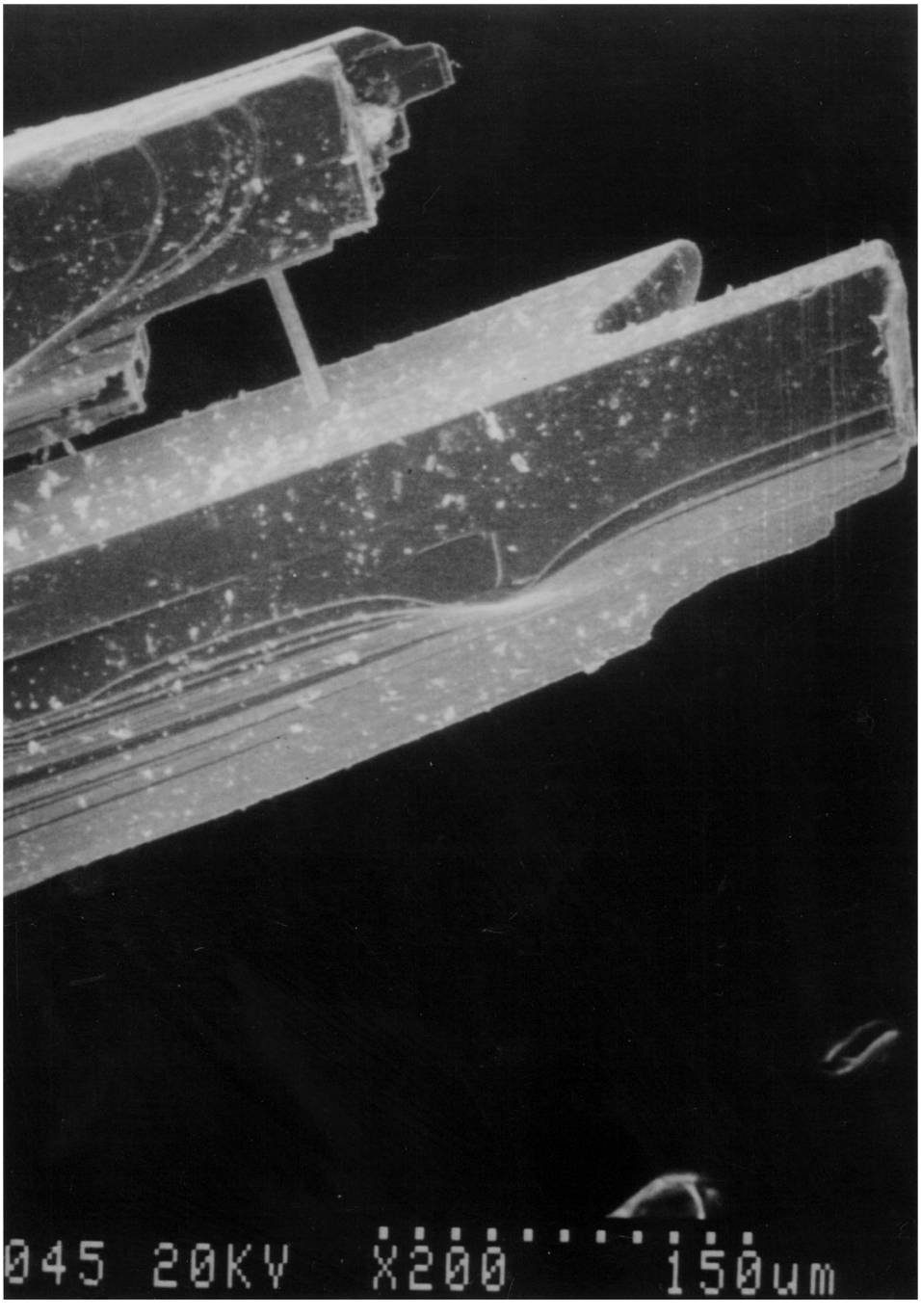

FIG. 5. Low-resolution electron micrograph of Mo_2N macrocrystal. Scale is indicated by dashed line in title bar.

is sloughed off as reduction progresses into the material. Reduction of the macrocrystalline MoO_3 could begin at the edge and progress inward, reducing the oxide to form a more dense phase. This could explain the thinness of the flat product compared to the layered zone which is consumed. After the reaction front had penetrated far enough into the macrocrystal, this phenomena could possibly allow for the product material to break away from the parent solid as a small platelet or flake.

Powder X-ray diffraction analysis of ground macrocrystals indicates the product of temperature programmed reaction to be γ-Mo_2N with traces of MoO_2 also present (20). The [200] peak of Mo_2N at 43.45° is more intense than the [111] peak at 37.5° as has been previously reported for high surface area Mo_2N powders produced by temperature programmed reaction (12). Scherrer analyses of Mo_2N diffraction peak widths indicate that the solid diffracting domains in the ground material average 4 or 5 nm in

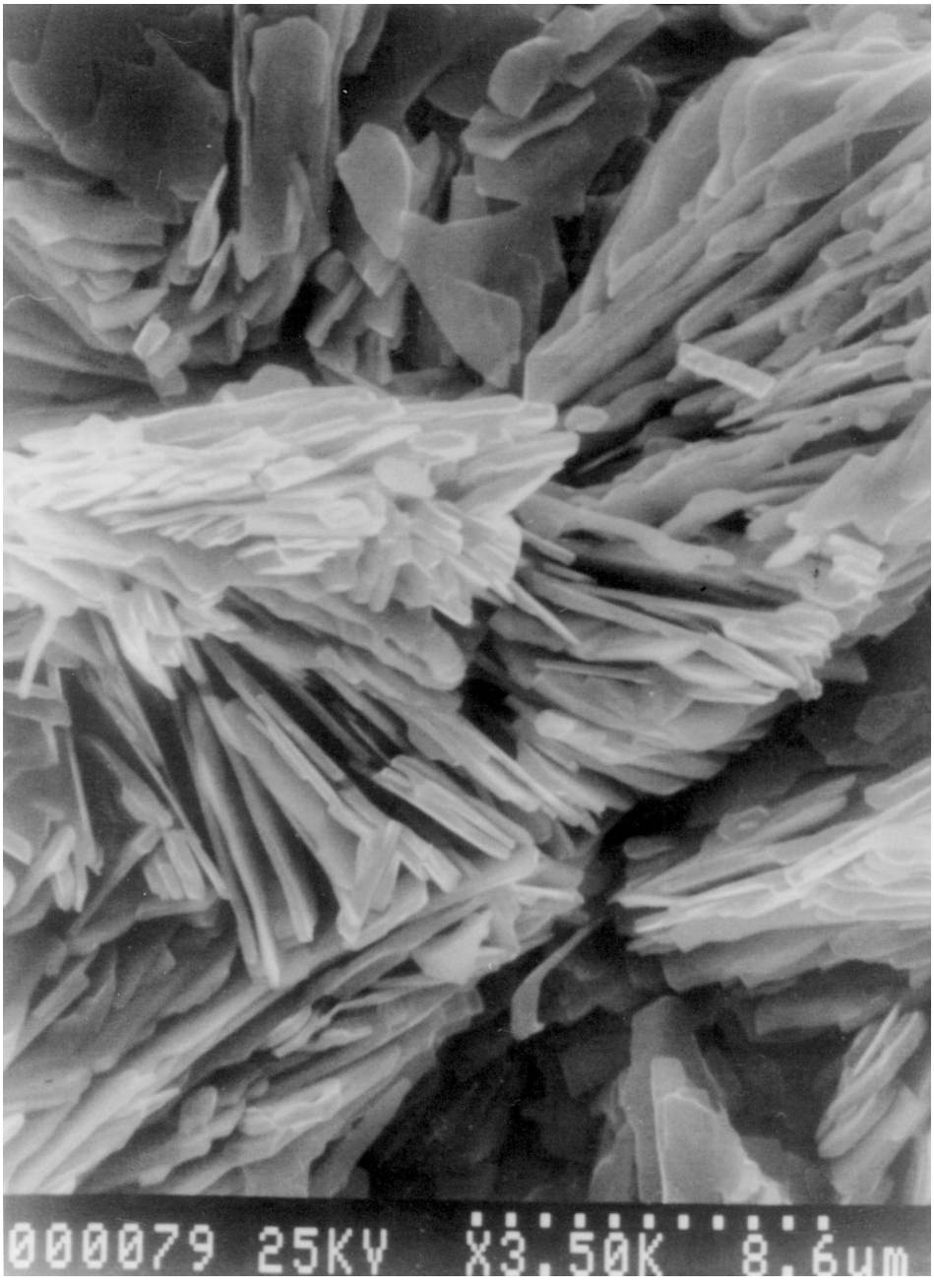

FIG. 6. High-resolution electron micrograph of Mo_2N flakes on macrocrystal surface. Scale is indicated by dashed line in title bar. Side view of two partially converted MoO_3 crystallites showing consumption of the starting material to form thin product layers which break off to form flakes.

diameter, depending on the lattice plane analyzed. Calculated particle diameters do not match because the Scherrer analysis assumes that the sample is composed of spherical crystalline Mo_2N. In practice, the sample may consist of nonspherical polycrystalline particles with a partially amorphous surface phase. It is notable that the crystalline dimensions perpendicular to the [200] axis are consistently shorter than the [111] direction. This result was observed previously in Mo_2N powders. For this reason, the morphology of the nanocrystallites which make up the Mo_2N macrocrystals are like the much larger bulk crystals and flakes: each is thinner in the [200] direction than in the [111] direction.

X-ray diffraction scans of oriented Mo_2N macrocrystals are shown in Fig. 7. If the small solid domains which make up the crystal were randomly oriented, these patterns would be identical to the powder pattern obtained from the ground macrocrystal sample. However, the diffraction patterns exhibit only one strong peak corresponding to the (200), (020), and (002) planes. This result would indicate that the Mo_2N macrocrystals consist of small solid diffracting

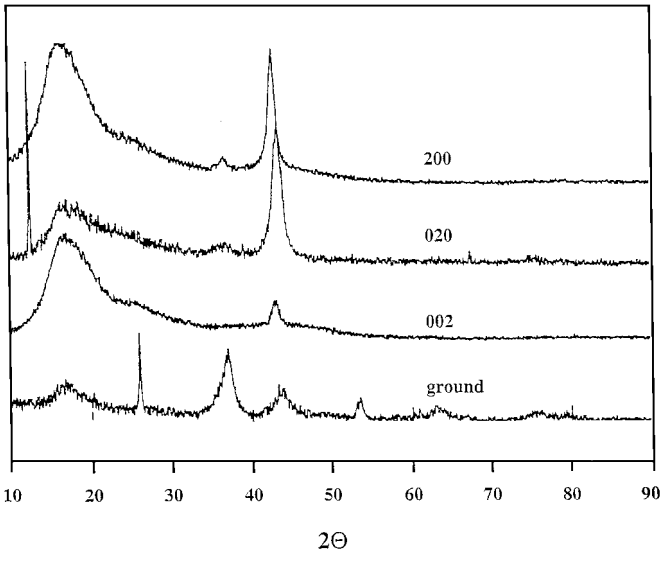

FIG. 7. One-dimensional X-ray diffraction patterns produced by oriented macrocrystals of Mo_2N as well as the same macrocrystal ground to a powder.

domains 4–5 nm in diameter in crystallographic alignment. Previous work by Volpe and Boudart has examined the synthesis of Mo_2N from the reaction of NH_3 with MoO_3 powders and crystalline platelets and has determined that the temperature programmed reaction is topotactic (1). Topotactic reactions are defined to occur when a solid product has well-defined crystallographically orientation relative to the starting (or parent) solid. The MoO_2 observed in the ground sample has a low specific surface area, as evidenced by its narrow diffraction peaks, and integration of the observed peaks indicates that MoO_2 is present in only trace amounts (20). Only a single peak at 13° is observed from macrocrystalline Mo_2N, instead of the series of peaks expected for a random arrangement of particles.

Scanning tunneling microscopy (STM) was employed to investigate both the structure of the solid domains as well as the pore structure of these materials in Fig. 8. STM of the [200] face of the topotactic macrocrystal synthesized by reaction of MoO_3 and NH_3 shows that the product consists of rounded particle sizes calculated from X-ray diffraction peak widths. The measured surface area (44 m^2/g) of

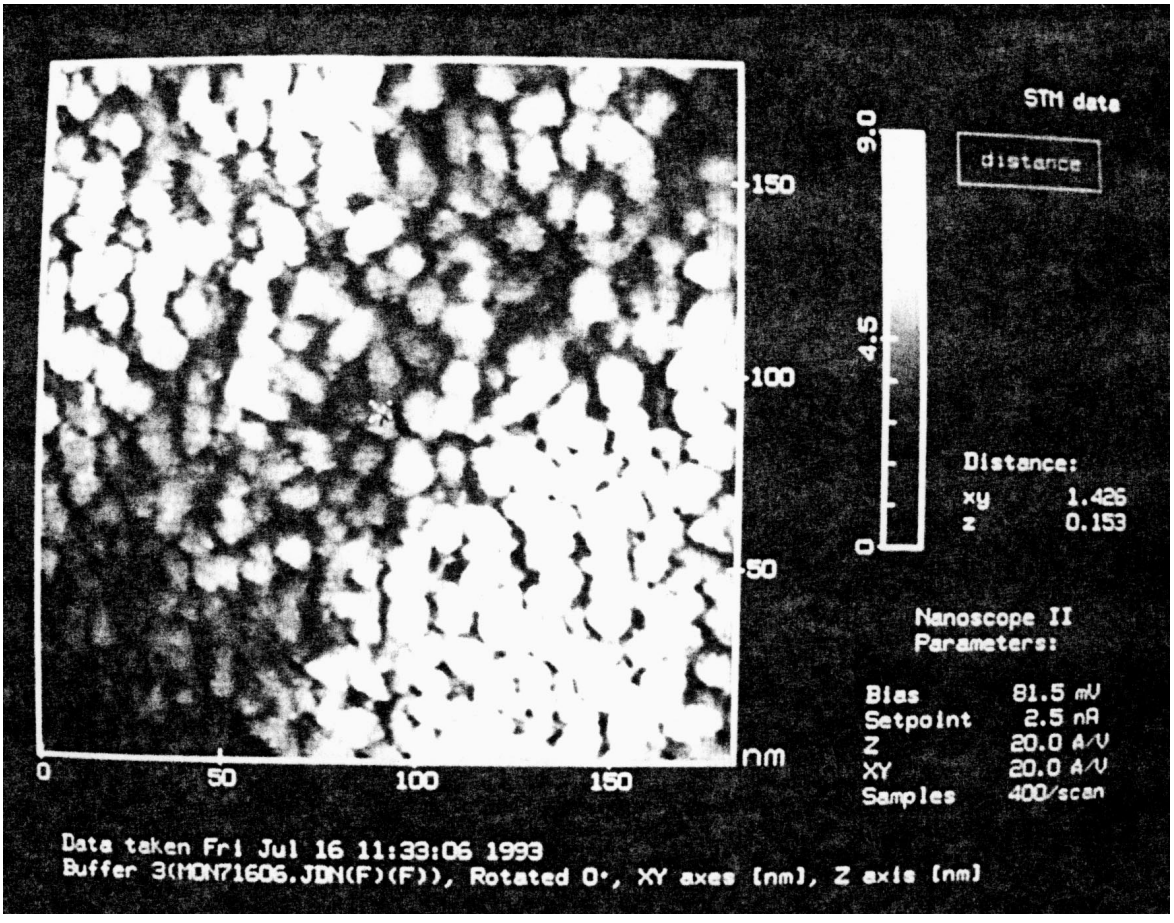

FIG. 8. Scanning tunneling micrograph of Mo_2N macrocrystal (200) plane from [5].

the macrocrystal points to an average particle diameter of 13 nm. Based on diffraction data, STM measurements, and surface area measurements, it is concluded that the particles are found with a range of diameters from 4 to 13 nm, flattened in the [200] direction with either an amorphous surface phase or polycrystalline interior to account for the small Scherrer diameters observed. It was not possible to achieve atomic resolution using these samples, although such imaging would be useful for verifying the crystallographic alignments of individual particles.

Thiophene desulfurization kinetic measurements. Thiophene desulfurization activity over 0.1 g of γ-Mo_2N macrocrystals was measured at 400°C over a 12-h period. The catalyst deactivates 30% during approximately the first 4 h of reaction but maintains a relatively constant level of activity after that time of approximately 36.1% thiophene conversion. The principle products of thiophene desulfurization were identified by GC/MS as C_4 hydrocarbons: butadiene, 1-butene, *cis*-2-butene, *trans*-2-butene, and butane. Smaller amounts of C_2 products were also observed. Product selectivities at 400°C throughout the 12-h reaction period as well as selectivities measured at high space velocities are plotted as a function of fractional conversion of thiophene (Fig. 9). Fractional selectivities for butane, butadiene, and butene are strong functions of the thiophene fractional conversion.

In all cases, the observed principle product (>55%) of desulfurization is butene. Smaller amounts of butane (10–45%) and even lesser quantities (<3.5%) of butadiene are also observed. Interestingly, the dominant product expected at equilibrium is butane (26, 27), but only a fraction of the product is observed as butane in these kinetic experiments. The observed product distributions are, therefore, due to reaction kinetics.

At higher thiophene conversions, the isomerization and hydrogenation reactions appear to be nearly at

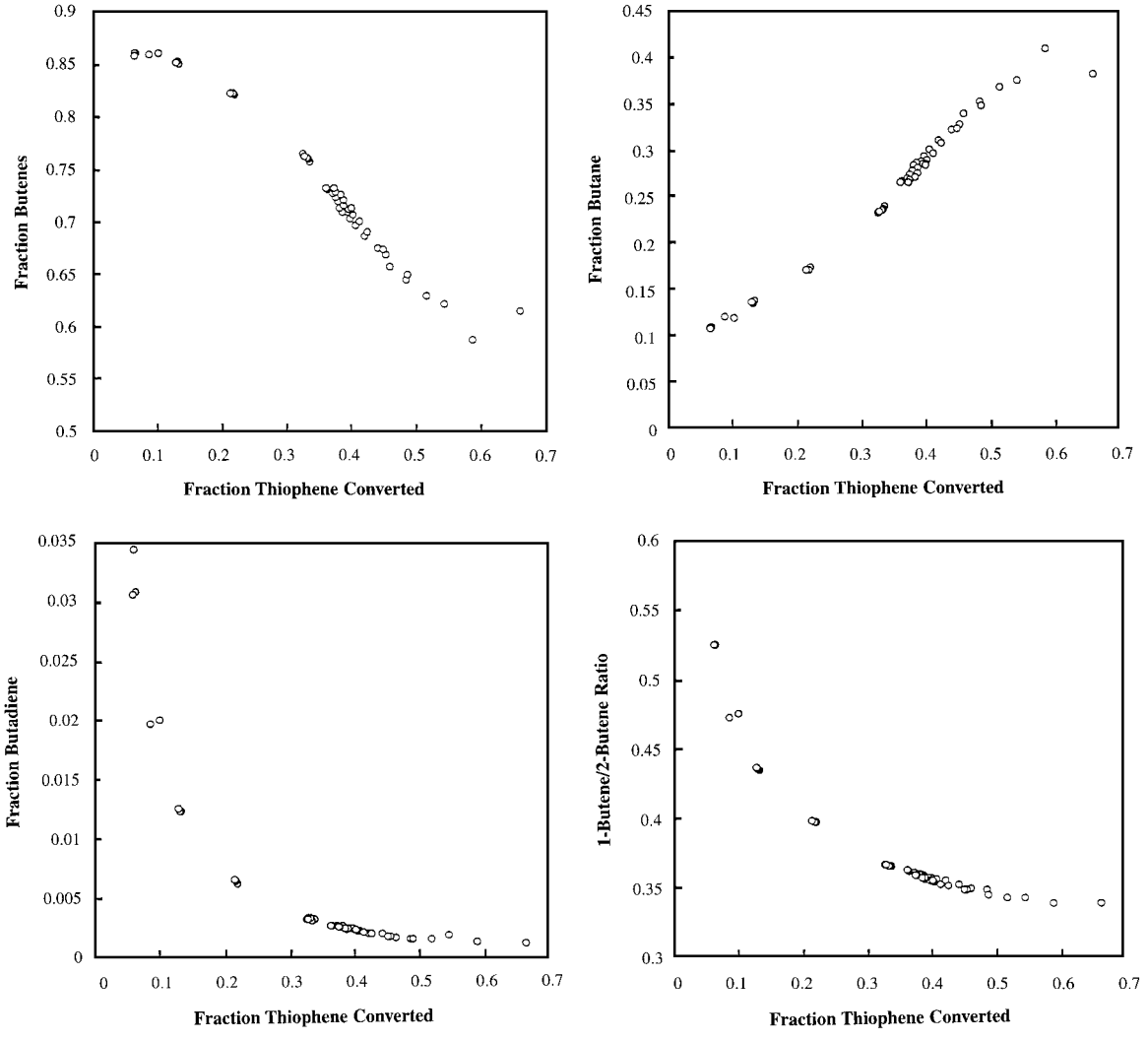

FIG. 9. Thiophene desulfurization product selectivities. (a) Butenes, (b) butane, (c) butadiene, and (d) 1-butene/2-butene ratio.

equilibrium with the exception of the butene hydrogenation reaction. The butenes are present in thermodynamic equilibrium amounts (a *cis*/*trans*-2-butene ratio of 0.702 and a 1-butene/2-butene ratio of 0.35) and very little butadiene is present, as predicted by thermodynamics. However, the majority of the products are butenes over the range of conversions observed in this work and these are only slowly hydrogenated to butane.

At differential conversions, 1-butene is the predominant product of thiophene desulfurization. Extrapolation of selectivities to zero conversion indicates the direct product of thiophene desulfurization is 1-butene with lesser amounts of 2-butenes formed and less than 10% of reacted thiophene converted to butane. The amount of butadiene produced directly from thiophene is not known because its selectivity curve is asymptotic to the vertical axis, but it is clear that a significant amount of butadiene is produced directly from thiophene. Changes in selectivities as the fractional thiophene conversion increases are not due to the kinetics of the thiophene desulfurization reaction, but rather the kinetics of the concurrent C_4 hydrogenation and isomerization reactions. Even at differential conversions, the *cis* and *trans* isomers of 2-butene are in equilibrium with *cis*/*trans* ratio of 0.702.

DISCUSSION

Proposed structures of high surface area topotactic metallic materials have ranged from highly ordered crystalline structures (similar to zeolites, consistent with the ordered structural changes expected from topotactic reaction) to disordered structures (5). In addition, three-dimensional pore structures or two-dimensional, layered pore structures are possible. Previous efforts to investigate the pores and solid structure of topotactic Mo_2N powders by electron microscopies and probe microscopies (e.g., STM and atomic force microscopies) did not produce acceptable images of sample topography. Scanning tunneling microscopic images of topotactic macrocrystalline Mo_2N show the topotactic material is an aggregate of rounded particles (Fig. 8). In addition, X-ray diffraction data show the particles are in crystallographic alignment (Fig. 3). This suggests that the particles are interconnected into locked positions relative to one another to form porous macrocrystals of γ-Mo_2N.

The topotactic reaction kinetics of crystalline Mo_2N synthesis are unlike that for the synthesis of Mo_2N powder. TGA data from this work indicate the rate of the reduction reaction is slower for larger crystals than a fine powder, consistent with a solid-state diffusion limited reaction. Previous work with powders has shown that the activation energy of the synthesis of Mo_2N from MoO_3 is comparable with systems involving the solid-state diffusion of oxygen in metal oxides (28). TGA data also show that a very slow temperature ramping rate is required for reduction to commence at low temperature. This result is observed in both the crystalline and the powder systems.

Scanning electron microscopy images from the work of Volpe and Boudart have shown that the reduction of platelets of MoO_3 powder less than 10 μm thick commences at the platelet edges, consuming a portion of the layered oxide and forming a reduced product which has the same thin layer morphology but is considerably thinner than the zone of the oxide which is consumed (1). After a period of reaction, the product material appears to break away from the oxide to form product flakes. It is possible that similar morphology changes occur during the reduction of the macrocrystals, except the product was not observed to separate from the initial MoO_3 macrocrystals. This route is consistent with the gross observation of macrocrystal oxide samples darkening first occurring at the edge of the crystal. Similar phenomena have previously been observed by Volpe and Boudart for the treatment of MoO_3 platelets in NH_3 below 620 K (1). It is possible that the product layers are stabilized or held in place by layers both above and below in single crystal reactions so that individual product layers do not readily break off as flakes. In this way, the product of reaction consists of a mat of loosely bound Mo_2N layers less than 200 nm thick. Each layer is porous with most of the observed surface area located in these pores, not the exposed basal planes of each layer. This porous mat can be peeled easily to expose interior surfaces for analysis.

High hydrogen concentrations are required to reduce the crystals at low temperatures and generate surface area. It is not clear why relatively modest changes in hydrogen concentrations (e.g., dropping from 75 to 30%) affect the reduction reaction strongly. Equilibrium effects are not responsible for the observed effects of concentration on reaction: for all gas phase compositions used in this study, the equilibrium solid phase is MoO_2, Mo_2N, or Mo. No MoO_3 is expected at equilibrium. Thus, hydrogen concentration has a strong effect on reaction kinetics, perhaps due to competitive adsorption effects. It has been shown that H_2O has a strong effect on reduction kinetics in the powder system at concentrations as low as 1000 ppm due to competitive adsorption effects (7). High gas space velocities are required in these syntheses because the H_2O produced by reaction must be rapidly purged from the bed.

The specific thiophene desulfurization activity of the crystalline Mo_2N is 2.5 times higher than the activity of the powder (Table 2). The origin of this higher activity is not known but has been observed previously by this group for study of thiophene desulfurization by Mo_2N in powder form with varying surface areas (12). This augmentation in activity for the low surface area nitrided molybdenum powdered catalysts was attributed to the presence of MoN, which was detected using X-ray diffractometry. This result suggested that differences in oxidation state between MoN (+3) and

TABLE 2

Summary of Measured Thiophene Desulfurization Activities at 400°C and Activities of Reference Compounds

Compound	Surface area (m^2/g)	Thiophene conversion (%)	Activity (mol/s m^2)
Powder Mo_2N (ref. 12)	108	38.1	1.95
Macrocrystalline Mo_2N	44	36.1	4.54
MoS_2 (ref. 27)	3.4	0.76	0.92
$Co_{0.25}MoS$ (ref. 27)	10.83	0.77	2.92
$Co_{1.5}Mo_6S_8$ (ref. 27)	0.15	0.54	0.82

Mo_2N (+2.5) could in some way influence the activity of molybdenum nitride catalysts. Daage and Chianelli have also reported catalyst structure effects for the hydrogenation and hydrodesulfurization of dibenzothiophene (DBT) over Mo_2S powders and microcrystals (14). The work of Daage and Chianelli reported that both hydrogenation and hydrodesulfurization were catalyzed over Mo_2S powders, while only the HDS of dibenzothiophene was catalyzed over Mo_2S microcrystals. Daage and Chianelli explained these results using a "rim-edge" model which attributed the microcrystalline Mo_2S catalyst selectivity for the HDS reaction to the ratio of exposed basal planes to covered basal planes for layered Mo_2S catalyst particles. Sites located at the edges of the exposed layers were named rim sites and those at the edges of interposing catalyst particle layers were called edge sites. These Mo_2S rim/edge site ratios were correlated to the optical defect density of each catalyst using photodeflection spectroscopy (PDS). Thompson and coworkers observed similar trends in pyridine HDN reactions and found that activity normalized more readily using oxygen uptake values for unsupported catalysts with compositions similar to those of working catalysts (29).

The observed trends in C_4 selectivities are similar to those observed previously for Mo_2N powders (12). Based on selectivity trends at low conversions, it is possible to identify those C_4 products produced directly from thiophene and trends at higher conversions can be used to qualitatively understand hydrogenation and isomerization reactions which accompany the desired desulfurization reaction (Fig. 10). Desulfurization of thiophene produces primarily 1-butene along with lesser amounts of 2-butenes, butane, and butadiene. Before 20% thiophene conversion is reached, the butene isomers are converted to an equilibrium distribution of isomers (and *cis*- and *trans*-2-butene isomers remain in equilibrium ratios at all levels of thiophene conversion). Butadiene reacts rapidly with the vast excess of hydrogen and is found only at relatively low fractions below 5% at moderate thiophene conversions. Butene is hydrogenated relatively slowly to form butane. If allowed to proceed to equilibrium, all products would be converted to butane except for traces of butenes and even smaller amounts of butadiene (27).

The predominance of 1-butene as a direct product of thiophene desulfurization has been observed in a number of other systems (12, 30–33). Although the overall observed butadiene content was observed to be less than 1% at low thiophene conversions (<10%), the upper limit of butadiene selectivity was not measured in this work and could have possibly affected the observed product fractions at very low thiophene conversions (<1%). Formation of butene from thiophene requires a desulfurization mechanism in which four hydrogen atoms are transferred to the carbon backbone before elimination of sulfur. Most proposed mechanisms involve a sequence of two hydrogenolysis steps and two hydrogenation steps in any of a number of combinations. An analysis of the possible combinations of these four steps shows that many are inconsistent with the observation of 1-butene as the predominant product. For example, two successive hydrogenolysis steps will lead to butadiene as the direct product of reaction. Other combinations lead to high-energy intermediates or high-energy products which are expected to be extremely reactive and should not be observed in significant quantity in the gas phase or the surface. Two combinations which would lead to the formation of 1-butene involve (i) two hydrogenation steps to form a 2,3-dihydrothiophene followed by two hydrogenolysis steps and (ii) a hydrogenolysis step followed by a double hydrogenation of the dangling C_4 chain and eventual cleavage to form free 1-butene. Combination (i) is considered less likely because work with dihydrothiophenes has shown that 2,3-dihydrothiophene and 2,5-dihydrothiophene rapidly isomerize under these reaction conditions, leading to the formation of *cis*-2-butene in excess of equilibrium, which was not observed (34, 35). For this reason, the most likely path for desulfurization involves hydrogenolysis of a single C–S bond, followed by a dual hydrogenation of the dangling diene chain, followed by hydrogenolysis of the remaining C–S bond to yield predominantly 1-butene.

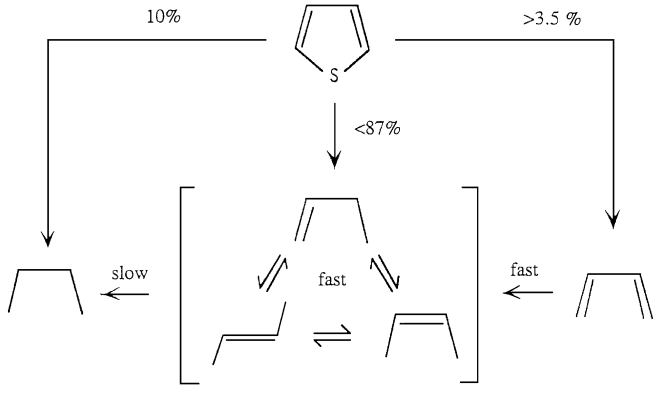

FIG. 10. Proposed thiophene desulfurization reaction pathway (Mo_2N macrocrystal).

CONCLUSIONS

Macrocrystalline Mo_2N has been synthesized from MoO_3 macrocrystals by temperature programmed reaction in N_2/H_2 and NH_3 gases. In this work, Mo_2N macrocrystals were revealed to have a specific surface area of 44 m^2/g. γ-Mo_2N macrocrystals are relatively small, dark metallic-gray platelets of moderately porous material which have visible dimensions varying from micrometer- to centimeter-scaled proportions.

From scanning electron microscopic analyses, the synthesis reaction appears to commence at the edges of the planar MoO_3 macrocrystals and later convert the crystalline MoO_3 into a mat of layers each less than 200 nm thick. However, the bulk of the porosity of the Mo_2N macrocrystals does not appear to be located in these exposed basal planes, but instead in a fine pore structure. Scanning tunneling microscopy and X-ray diffraction shows that the solid consists of Mo_2N crystallites which are foreshortened in the [200] direction with either an amorphous surface phase or a polycrystalline core. X-ray diffraction patterns from Mo_2N macrocrystals indicate the presence of crystallites which are locked in crystallographic alignment. TGA analyses of the reduction/nitridation reaction indicate that the reaction is slower in the macrocrystalline than equivalent powder syntheses. The rate of reaction is likely limited by solid-state diffusion where the reduction reaction would possibly commence at the edges of the MoO_3 macrocrystal and consume the oxide from the edges inward.

The thiophene desulfurization activity of macrocrystalline Mo_2N is observed to be more than twice that of Mo_2N powder on an area basis but is of equal activity on a mass basis. The reason for this difference in area specific activities is unknown. Product selectivities for butenes, butane, and butadiene for the thiophene desulfurization over Mo_2N macrocrystal catalysts are in close agreement with those observed for Mo_2N powder catalysts. Thiophene is desulfurized to form predominantly 1-butene with smaller amounts of other C_4 compounds observed.

ACKNOWLEDGMENTS

This work was supported by the National Science Foundation Grant OFR-9108772-02. The National Science Foundation also provided funding for the electron microscope (Equipment Grant DIR-9016370). K. L. Roberts also thanks the Department of Energy EPSCoR Fellowship program at the University of South Carolina and the Department of Energy Samuel Massie Chair of Excellence in Environmental Engineering at North Carolina Agricultural and Technical State University for their support of this work. We also thank Professor Michael Myrick of the Department of Chemistry at the University of South Carolina for assistance with the scanning tunneling microscopic analyses and Dr. Dana Dunkelberger of the Electron Microscopy Center at the University of South Carolina for assistance with the scanning and transmission electron microscopic analyses.

REFERENCES

1. Volpe, L., and Boudart, M., *J. Solid State Chem.* **59**, 332 (1985).
2. Ranhorta, G. S., Haddix, G. W., Bell, A. T., and Reimer, J. A., *J. Catal.* **108**, 24 (1987).
3. Choi, J.-G., Curl, R. L., and Thompson, L. T., *J. Catal.* **146**, 218 (1994).
4. Wise, R. S., and Markel, E. J., *J. Catal.* **145**, 335 (1994).
5. Roberts, K. L., and Markel, E. J., *J. Phys. Chem.* **98**, 4083 (1994).
6. Volpe, L., and Boudart, M., *J. Phys. Chem.* **90**, 4878 (1986).
7. Wise, R. S., and Markel, E. J., *J. Catal.* **145**, 344 (1994)
8. Ranhorta, G. S., Bell, A. T., and Reimer, J. A., *J. Catal.* **108**, 40 (1987).
9. Oyama, S. T., *Catal. Today* **15**, 279 (1992).
10. Schlatter, J. C., Oyama, S. T., Metcalfe, J. E., and Lambert, J. M., *Ind. Eng. Chem. Res.* **27**, 1648 (1988).
11. Choi, J.-G., Brenner, J. R., Colling, C. W., Demczyk, B. G., Dunning, J. L., and Thompson, L. T., *Catal. Today* **15**, 201 (1992).
12. Markel, E. J., and Van Zee, J. W., *J. Catal.* **126**, 643 (1990).
13. Nagai, M., Miyao, J., and Tsuboi, T., *Catal. Lett.* **18**, 9 (1993).
14. Daage, M., and Chianelli, R. R., *J. Catal.* **149**, 414 (1994).
15. Bertrand, O., and Dufour, L. C., *Phys. Status Solidi A* **60**, 507 (1980).
16. Anderson, J., *J. Physique, Suppl.* **38**, C7–C17 (1977).
17. Hillis, M. R., Kemball, C., and Roberts, M. W., *Trans. Faraday Soc.* **62**, 3570 (1966).
18. King, E. G., Weller, W. W., and Christensen, A. U., U.S. Bur. Mines, Report, 1960.
19. Bursill, L. A., *Proc. R. Soc. A* **311**, 267 (1969).
20. JCPDS X-ray Powder Diffraction Inorganic Reference Data, 1987.
21. Gusev, A. I., *Phys. Stat. Sol. (B)* **163**, 17 (1991).
22. Wise, R., and Markel, E., unpublished results.
23. Klug, H. P., and Alexander, L. E., *in* "X-Ray Diffraction Procedures," p. 511. Wiley, New York, 1962.
24. Colling, C. W., Choi, J.-G., and Thompson, L. T., *J. Catal.* **160**, 35 (1996).
25. Burdick, S. E., and Markel, E. J., unpublished results.
26. Benson, S. W., and Bose, A. W., *J. Am. Chem. Soc.* **85**, 1385 (1963).
27. Chase, M. W., Davies, C. A., Downey, J. R., Frurip, D. J., McDonald, R. A., and Syverud, A. N., JANAF Thermochemical Tables, 3rd ed.
28. Oyama, S. T., Schlatter, J. C., Metcalfe, J. E., and Lambert, J. M., *Ind. Eng. Chem. Res.* **27**, 1639 (1988).
29. Choi, J.-G., Brenner, J. R., Colling, C. W., Demczyk, B., Dunning, J. L., and Thompson, L. T., *Catal. Today* **15**, 201 (1992).
30. McCarty, K. F., Anderegg, J. W., and Schrader, G. L., *J. Catal.* **93**, 375 (1985).
31. Osbaldiston, R. J. C., MS thesis, Univ. of South Carolina, 1993.
32. Desikan, P., and Amberg, C. H., *Can. J. Chem.* **41**, 1966 (1963).
33. Kolboe, S., and Amberg, C. H., *Can. J. Chem.* **44**, 2623 (1966).
34. Markel, E. J., Sauer, N. N., Angelici, R. J., and Schrader, G. L., *J. Catal.* **116**, 11 (1989).
35. Sauer, N. N., Markel, E. J., Schrader, G. L., and Angelici, R. J., *J. Catal.* **117**, 295 (1989).